Supplementary information

# $CH_3NH_3^+$ and Pb Immobilization Through $PbI_2$ Binding by Organic Molecule Doping for Homogeneous Organometal Halide Perovskite films

He Jiang [a,b,c], Qianqian Yao [a,b,c], Xiaoyue Zhang [a,b,c], Bangmin Zhang [a,b,c], Weiwei Xing [a,b,c], Yijing Sun [a,b,c], Weiming Xiong [a,b,c], Xin Luo [a,b,c], Wenpeng Zhu [a,b,c,*], Yue Zheng [a,b,c,*]

[a] Guangdong Provincial Key Laboratory of Magnetoelectric Physics and Devices, School of Physics, Sun Yat-sen University, Guangzhou 510275, China

[b] State Key Laboratory of Optoelectronic Materials and Technologies, School of Physics, Sun Yat-sen University, Guangzhou 510275, China

[c] Centre for Physical Mechanics and Biophysics, School of Physics, Sun Yat-sen University, Guangzhou 510275, China

[*] Corresponding authors:

E-mail address: zhuwp3@mail.sysu.edu.cn (Wenpeng Zhu)

E-mail address: zhengy35@mail.sysu.edu.cn (Yue Zheng)

This file of Supplementary information includes:

## Supplementary Notes

- Experimental Methods
- DFT Methods

## Supplementary Tables



## Supplementary Figures

films.

- Fig. S13. *J-V* characteristics with reverse and forward scans for PSCs based on undoped and PCBM+PMMA doped $MAPbI_3$ films.
- Fig. S14. Statistics of photovoltaic performance for PSCs based on undoped and PCBM+PMMA doped $MAPbI_3$ films.
- Fig. S15. Stability of unencapsulated PSCs based on undoped and PCBM+PMMA doped $MAPbI_3$ films

## Supplementary References

# Supplementary Notes

## 1. Experimental Methods

### 1.1 Materials

MAI (≥99%) and PMMA (average Mw~120,000) were purchased from Sigma-Aldrich. PCBM (>99.5%) and Spiro-OMeTAD (>99%) were purchased from Lumtec. $PbI_2$ (99.9985%) and $SnO_2$ colloidal precursor (tin (IV) oxide, 15% in $H_2O$ colloidal dispersion) were purchased from Alfa Aesar. N,N-Dimethylformamide (DMF, 99.8%, Extra Dry), dimethyl sulfoxide (DMSO, >99.7%, Extra Dry) and chlorobenzene (CB, 99.8%, Extra Dry) solvents were purchased from Acros Organics. All materials were used without further purification.

For $MAPbI_3$ perovskite precursor solutions (40 wt%), $PbI_2$ and MAI were dissolved in DMF and DMSO mixed solution (2:1 v/v) with a molar ratio of 1:1, and then stirred at 60°C for 8 h in glovebox. The CB solution with PCBM, PMMA or PCBM+PMMA for doping was prepared with a total mass concentration of 0.1 wt%. $SnO_2$ precursor solution was prepared by diluting purchased $SnO_2$ colloidal precursor with $H_2O$ (5:1 v/v). The synthesis method of Spiro-OMeTAD precursor solution is based on the previous literature.[1]

### 1.2 Film fabrications and characterizations

All the undoped and doped $MAPbI_3$ films were prepared on the substrates of FTO-coated glass by a one-step solution process using spin-coating method with anti-solvent method. The prepared $MAPbI_3$ precursor solution was dropped on the FTO substrate by the spin-coating method with an initial speed of 3000 rpm and an acceleration rate of 2000 rpm/s for 35 s. The anti-solvent method was applied during the spin coating, in which a small amount (150-200 μL) of CB solutions was dropped on the spinning substrate during the last 10 s. The doped $MAPbI_3$ films were obtained by using the CB solution with PCBM, PMMA or PCBM+PMMA.

The XPS C core-level and valance band spectra were obtained by using an ESCALAB 250 (Thermo-VG Scientific). The PL decay of $MAPbI_3$ films was studied by a FLS980

Spectrometer (Edinburgh) in air at room temperature. The $MAPbI_3$ films were photoexcited using a laser head (EPL-405) with a wavelength of 406.2 nm and a pulse width of 58.8 ps. The crystalline structures of $MAPbI_3$ films were obtained by XRD (D-MAX 2200 VPC) with a Cu-Kα radiation operated at 40 kV and 26 mA. The chemical mappings were obtained by nano-IR2 (Anasys Instruments) equipped with a pulsed quantum cascade laser (913-1900 $cm^{-1}$). The laser power was set as 67.57% with the pulse rate of ~300 kHz to enhance IR signal. The surface topography and chemical mappings were collected simultaneously by AFM-IR with a tapping mode using an Au-coated NIR2 probe (Anasys, PR-EX-TnIR-A-10) with a force constant of 1-7 nN/nm and a frequency of ~75 kHz. The FTIR spectra were obtained by an infrared spectrometer (Frontier). The SEM images were obtained by Quanta 250FEG (FEI). The SKPM measurements were performed in air using a Scanning Probe Microscope (MFP-3D Asylum Research). The surface potential images were collected by a tapping mode using a sharp conductive single crystal diamond probe (Adama, Au coating, 2.8 N/m, 65 kHz). The UV-Vis absorption spectra were measured using an UV-VIS-NIR spectrophotometer (UV 3600).

**1.3 Solar cell device fabrications and measurements**

FTO-coated glass substrate (NSG, 14 (±1.5) Ω/sq, T>85 %, 20*20 mm) was washed using cleaning powder, cleaned successively with ethyl alcohol, acetone, isopropanol and deionized water in an ultrasonic bath for 15 min each, and finally flushed with nitrogen. After UV-ozone surface treatment for 30 min, a $SnO_2$ thin-film was deposited onto the cleaned FTO substrate by using spin-coating method (3000 rpm for 30 s), and afterwards annealed at 150°C for 30 min on a heating plate in air. After cooling down to room temperature, the $SnO_2$-coated FTO substrate was treated by UV-ozone for 5 min and transferred to glovebox. The PCBM (2 wt % in CB solvent) layer was spin-coated (3000 rpm 30 s) onto the $SnO_2$-coated FTO, and then annealed at 110 °C for 30 min. The prepared $MAPbI_3$ precursor solution was dropped on the FTO/$SnO_2$/PCBM substrate by the spin-coating method with an initial speed of 3000 rpm and

an acceleration rate of 2000 rpm/s for 35 s. The anti-solvent method was applied during the spin coating of the $MAPbI_3$ layer, in which a small amount (150-200 μL) of CB solutions was dropped on the spinning substrate during the last 10 s of the spin-coating process. The doped $MAPbI_3$ layers were obtained by using the CB solution with PCBM, PMMA or PCBM+PMMA. After spin-coating, the FTO/$SnO_2$/PCBM/$MAPbI_3$ substrate was put on a heating plate at 100 °C for 40 min. Spiro-OMeTAD as the hole transfer layer was coated on $MAPbI_3$ with a spin speed of 3000 rpm for 30 s, without further annealing treatment. A 40 nm Au (99.999%) layer was eventually deposited by thermal evaporation with a metal pattern plate to form the planar PSCs with the configurations of FTO/$SnO_2$/PCBM/perovskite/Spiro-OMeTAD/Au.

The *J-V* characteristics of PSC devices were obtained by using a Keithley 2400 Semiconductor Characterization System under the illumination of one-sun AM1.5G (100 $mW/cm^2$) solar simulator (Abet Technologies Sun 3000). The light intensity was calibrated by a KG-5 crystalline silicon diode. A shadow mask (circular aperture, 0.07 $cm^2$) was used for the calibration of the active area. A voltage step of 30 mV was fixed in the reverse scans (from 1.2 V to -0.2 V) and the forward scans (from -0.2 V to 1.2 V). The EQE spectra were obtained by using a quantum efficiency measurement system QEXL (PV measurements), and calibrated by a standard single-crystal silicon reference cell. All the device measurements were carried out in air conditions.

**2. DFT Methods**

Density functional theory (DFT) calculations were performed using the Vienna ab initio simulation package (VASP)[2] with the projector-augmented-wave (PAW)[3] approach. The exchange–correlation contributions were considered via the Perdew-Burke-Ernzerhof (PBE)[4] functional within the generalized gradient approximation (GGA). The plane wave basis set-up to an energy cut-off of 500 eV was utilized throughout all the calculations. For the geometrical optimizations, the structures were allowed to relax until the total energy converged below $10^{-6}$

eV per atom and the forces converged below 0.01 eV $Å^{-1}$. Van der Waals forces were accounted for by applying the DFT-D3 method of Grimme.[5,6] $MAPbI_3$ with 1 × 1 × 2 supercell was employed in our calculations, which containing 48 atoms in the defect-free structure. A 6 × 6 × 4 Monkhorst-Pack k-point grid was used for the geometrical optimization and density of states, while 10 k-point paths between adjacent k-point along the high symmetry lines within the first Brillouin zone were used to generate the band structure. To visualize the atomic structures in DFT modeling, the atoms in $MAPbI_3$, PCBM, and PMMA are depicted as spheres and colored as follows: Carbon (C): brown; Nitrogen (N): blue; Hydrogen (H): white; Lead (Pb): gray; Iodine (I): purple; Oxygen (O): red.

The formation free energies for MA vacancy ($\Delta G_{V_{MA}}$) were calculated as

$$\Delta G_{V_{MA}} = \Delta E_{V_{MA}} + \Delta E_{ZPE} - T\Delta S$$

where $\Delta E_{V_{MA}}$ is the formation energy for MA vacancy, $\Delta E_{ZPE}$ and $\Delta S$ are the zero-point energy difference and entropy difference between the $MAPbI_3$ with MA vacancy and the defect-free $MAPbI_3$, and $T$ is the ambient temperature as 298.15 K. The formation energy for MA vacancy $\Delta E_{V_{MA}}$ was obtained by

$$\Delta E_{V_{MA}} = (E_{V_{n*MA}} + nE_{MAI}) - (E_{defect\text{-}free} + \frac{n}{2}E_{I_2(g)})$$

where *n* is the number of MA vacancies. The $E_{V_{n*MA}}$, $E_{MAI}$, $E_{defect\text{-}free}$, and $E_{I_2(g)}$ are the total energy of $MAPbI_3$ with the MA vacancies, the average unit energy of one MAI in bulk phase, the total energy of defect-free $MAPbI_3$, and the energy of an $I_2$ molecule in gas phase, respectively. As the vibrational frequency and entropy of crystal structure in the solid state are small, the difference in zero-point energy is $\Delta E_{ZPE} \approx -\frac{n}{2}E_{ZPE}^{I_2}$ and the entropy difference is $\Delta S \approx -\frac{n}{2}S_{I_2}^0$, where $E_{ZPE}^{I_2}$ is the zero point energy of the $I_2$ molecule in the gas phase, $S_{I_2}^0$ is the entropy of the $I_2$ molecule in the gas phase at the standard conditions.[7,8]

The formation free energies for Pb-occupied MA vacancy ($\Delta G_{\mathrm{Pb_{MA}}}$) were derived as

$$\Delta G_{\mathrm{Pb_{MA}}} = \Delta E_{\mathrm{Pb_{MA}}} + \Delta E_{\mathrm{ZPE}} - T\Delta S$$

where $\Delta E_{\mathrm{Pb_{MA}}}$ is the formation energy for Pb-occupied MA vacancy, $\Delta E_{\mathrm{ZPE}}$ and $\Delta S$ are the zero-point energy difference and entropy difference between $MAPbI_3$ with Pb-occupied MA vacancy and unoccupied MA vacancy, and $T$ is the ambient temperature as 298.15 K. The formation energy for Pb-occupied MA vacancy $\Delta E_{\mathrm{Pb_{MA}}}$ can be given as

$$\Delta E_{\mathrm{Pb_{MA}}} = (E_{\mathrm{n*Pb_{MA}}} + nE_{\mathrm{I_2(g)}}) - (E_{\mathrm{V_{n*MA}}} + nE_{\mathrm{PbI_2}})$$

where *n* is the number of Pb-occupied MA vacancies. The $E_{\mathrm{n*Pb_{MA}}}$, $E_{\mathrm{I_2(g)}}$, $E_{\mathrm{V_{n*MA}}}$, and $E_{\mathrm{PbI_2}}$ are the total energy of $MAPbI_3$ with Pb-occupied MA vacancies, the energy of an $I_2$ molecule in gas phase, the total energy of $MAPbI_3$ with MA vacancies, and the energy of $PbI_2$, respectively. As the vibrational frequency and entropy of crystal structure in the solid state are small, the difference in zero-point energy is $\Delta E_{\mathrm{ZPE}} \approx nE_{\mathrm{ZPE}}^{\mathrm{I_2}}$ and the entropy difference is $\Delta S \approx nS_{\mathrm{I_2}}^{0}$.

The binding free energies ($\Delta G_{\mathrm{binding}}$) of the interactions between the $PbI_2$ and the doped organic molecules (PCBM or PMMA) were defined as

$$\Delta G_{\mathrm{binding}} = \Delta E_{\mathrm{binding}} + \Delta E_{\mathrm{ZPE}} - T\Delta S$$

where $\Delta E_{\mathrm{binding}}$ is the binding energy, $\Delta E_{\mathrm{ZPE}}$ and $\Delta S$ are the zero-point energy difference and entropy difference, $T$ is the ambient temperature as 298.15 K. The binding energy $\Delta E_{\mathrm{binding}}$ for $PbI_2$ interacting with PCBM or PMMA can be given by

$$\Delta E_{\mathrm{binding}} = E_{\mathrm{PbI_2+PCBM/PMMA}} - E_{\mathrm{PCBM/PMMA}} - E_{\mathrm{PbI_2}}$$

where $E_{\mathrm{PbI_2+PCBM/PMMA}}$, $E_{\mathrm{PCBM/PMMA}}$, and $E_{\mathrm{PbI_2}}$ are the total energy of $PbI_2$ binding with PCBM or PMMA, the energy of PCBM or PMMA, and the energy of $PbI_2$, respectively. As $PbI_2$,

PCBM and PMMA are not in the gaseous form in $MAPbI_3$ films, the differences in vibrational frequencies and entropy are negligible, and hence $\Delta G_{\text{binding}} \approx \Delta E_{\text{binding}}$.

## Supplementary Tables

**Table S1.** Photoexcited carrier lifetime measured by PL decays of $MAPbI_3$ films. Different doping cases of "undoped", "PCBM doped", "PMMA doped" and "PCBM+PMMA doped" are studied. The mass ratios of 7:3, 1:1 and 3:7 between PCBM and PMMA are considered. Short lifetimes $\tau_1$ and long lifetimes $\tau_2$ associated with the corresponding relative amplitudes of $A_1$ and $A_2$ were obtained by fitting a bi-exponential equation as $Y(t)=A_1\exp(t/\tau_1)+A_2\exp(t/\tau_2)$. Average lifetimes were calculated by the equation of $\tau=A_1\tau_1+A_2\tau_2$. The mean standard deviations were derived from five independent samples of each case.

| | $A_1$ (%) | $\tau_1$ (ns) | $A_2$ (%) | $\tau_2$ (ns) | Average lifetimes $\tau$ (ns) |
|---|---|---|---|---|---|
| **Undoped** | 37 (±6) | 65 (±17) | 63 (±6) | 328 (±43) | 229 (±20) |
| **PCBM doped** | 17 (±11) | 146 (±65) | 83 (±11) | 696 (±36) | 599 (±39) |
| **PMMA doped** | 7 (±2) | 73 (±20) | 93 (±2) | 516 (±35) | 484 (±37) |
| **PCBM:PMMA =7:3 (w/w)** | 14 (±11) | 140 (±83) | 86 (±11) | 808 (±103) | 712 (±32) |
| **PCBM:PMMA =1:1(w/w)** | 14 (±6) | 166 (±66) | 86 (±6) | 892 (±104) | 788 (±73) |
| **PCBM:PMMA =3:7(w/w)** | 10 (±7) | 229 (±103) | 90 (±7) | 1183 (±132) | 1083 (±69) |

**Table S2.** Lattice constants, unit cell volumes and c/a values by fitting XRD patterns. The structural parameters of single-crystal $MAPbI_3$ originate from the work by Baikie, T. et al.[9]

| | **a (Å)** | **b (Å)** | **c (Å)** | **Unit Cell Volume ($Å^3$)** | **c/a** |
|---|---|---|---|---|---|
| **Single crystal[9]** | 8.8743 | 8.8743 | 12.6708 | 997.86605 | 1.42781 |
| **Undoped** | 8.86876 | 8.86876 | 12.61467 | 992.20504 | 1.42237 |
| **PCBM doped** | 8.87135 | 8.87135 | 12.62934 | 993.93936 | 1.42361 |
| **PMMA doped** | 8.87119 | 8.87119 | 12.62855 | 993.84245 | 1.42355 |
| **PCBM+PMMA doped** | 8.87214 | 8.87214 | 12.64694 | 995.50228 | 1.42547 |

**Table S3.** Formation free energy of one MA vacancy ($V_{MA}$) in $MAPbI_3$.

| **$MAPbI_3$ with one MA vacancy (eV)** | |
|---|---|
| **Defect free $MAPbI_3$** | -208.19 |
| **$V_{MA}$** | -166.01 |
| **MAI** | -42.29 |
| **0.5*$I_2$** | -1.32 |
| $\Delta E_{ZPE}$ | 0.01 |
| $T\Delta S$ | -0.40 |
| **Formation free energy** | 1.62 |
| **2*Formation free energy** | 3.24 |

**Table S4.** Formation free energy of two adjacent MA vacancies ($V_{2*MA}$) in $MAPbI_3$.

| **$MAPbI_3$ with two adjacent MA vacancy (eV)** | |
|---|---|
| **Defect free $MAPbI_3$** | -208.19 |
| **$V_{2*MA}$** | -123.75 |
| **2*MAI** | -84.58 |
| **$I_2$** | -2.65 |
| **$\Delta E_{ZPE}$** | 0.02 |
| **$T\Delta S$** | -0.80 |
| **Formation free energy** | 3.33 |

**Table S5**. Formation free energy of one Pb-occupied MA vacancy ($Pb_{MA}$) in $MAPbI_3$.

| **$MAPbI_3$ with one Pb-occupied MA vacancy (eV)** | |
|---|---|
| **$V_{MA}$** | -166.01 |
| **$Pb_{MA}$** | -170.38 |
| **$PbI_2$** | -7.39 |
| **$I_2$** | -2.65 |
| **$\Delta E_{ZPE}$** | -0.02 |
| **$T\Delta S$** | 0.80 |
| **Formation free energy** | -0.45 |
| **2*Formation free energy** | -0.90 |

**Table S6.** Formation free energy of two adjacent Pb-occupied MA vacancies ($Pb_{2*MA}$) in $MAPbI_3$.

| **$MAPbI_3$ with two adjacent MA vacancies occupied by Pb atoms (eV)** | |
|---|---|
| **$V_{2*MA}$** | -123.75 |
| **$Pb_{2*MA}$** | -133.93 |
| **$2*PbI_2$** | -14.78 |
| **$2*I_2$** | -5.30 |
| **$\Delta E_{ZPE}$** | -0.04 |
| **$T\Delta S$** | 1.60 |
| **Formation free energy** | -2.34 |

**Table S7.** Binding free energies for $PbI_2$ and doped organic molecules.

| | **Case 1: $PbI_2$ binding with PCBM (eV)** | **Case 2: $PbI_2$ binding with PMMA (eV)** |
|---|---|---|
| **PCBM/PMMA** | -704.21 | -87.63 |
| **$PbI_2$** | -7.39 | -7.39 |
| **PCBM/PMMA+$PbI_2$** | -712.19 | -95.55 |
| **Binding free energy** | -0.59 | -0.53 |

## Supplementary Figures

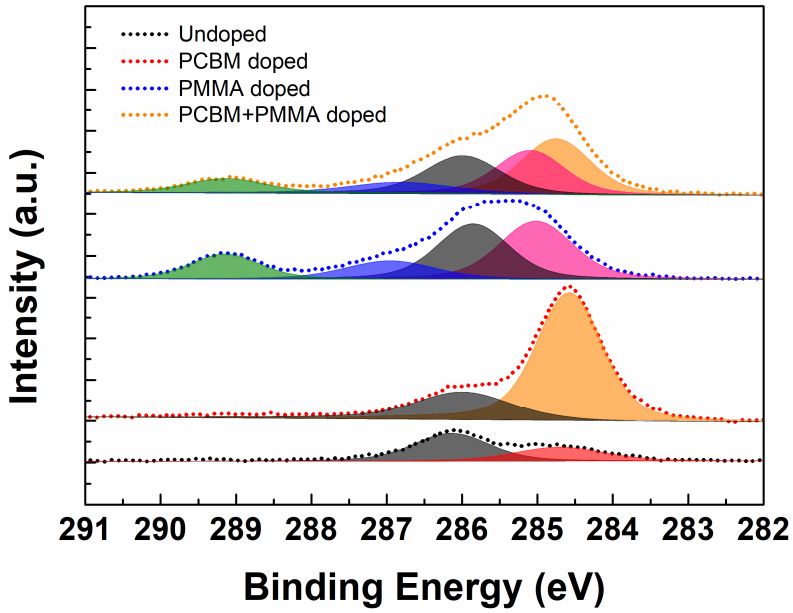


**Fig. S1.** XPS spectra of undoped and doped $MAPbI_3$ films. The carbon core-level spectra for MA state (~286 eV, black peak) in $MAPbI_3$ films, C-$CH_3$ (~285 eV, pink peak), O-$CH_3$ (286.8 eV, blue peak) and C-C=O (~289 eV, green peak) states in PMMA, and $C_{60}$ state (284.6 eV, orange peak) in PCBM are analyzed, which validate the distribution of PCBM and PMMA in the doped $MAPbI_3$ films.

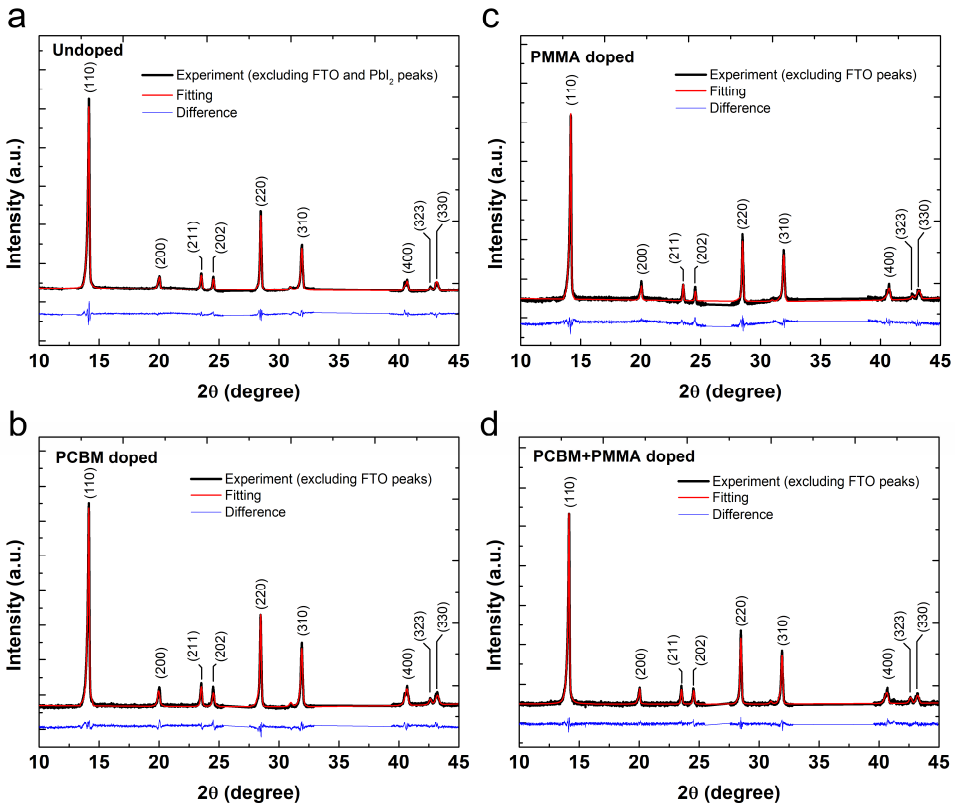


**Fig. S2.** GSAS fitting XRD patterns of undoped (a), PCBM doped (b), PMMA doped (c) and PCBM+PMMA doped (d) $MAPbI_3$ films. For fitting the structural parameters of $MAPbI_3$ films, nine XRD patterns for each doping case of $MAPbI_3$ films were selected with the peaks of $PbI_2$ and FTO excluded. The experimental XRD patterns and the fitting curves are plotted as the black and red curves, respectively. The blue curves show the differences between the experimental XRD patterns and the fitting curves.

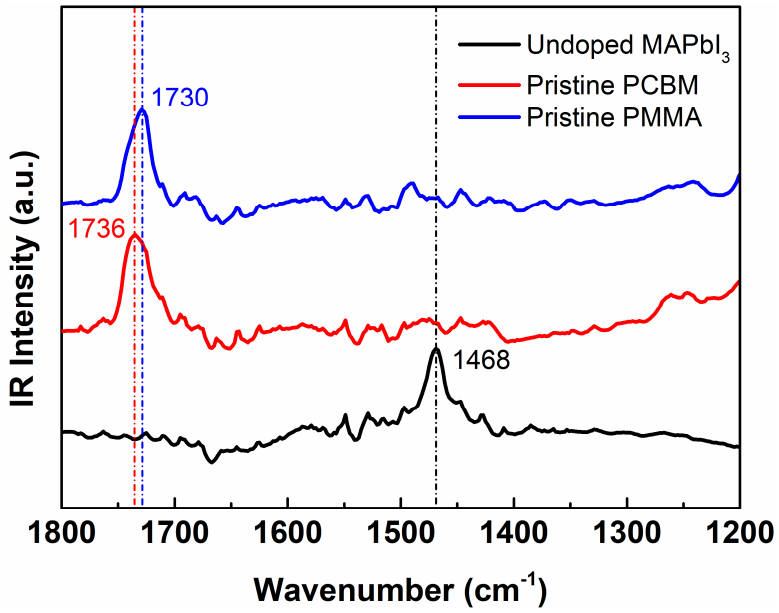


**Fig. S3.** Normalized IR spectra of undoped $MAPbI_3$ film, pristine PCBM and PMMA. The IR data was obtained by the contact-mode AFM-IR measurement. The characteristic IR peaks at 1468 $cm^{-1}$, 1736 $cm^{-1}$ and 1730 $cm^{-1}$, which correspond to the C-H bending of MA cations, the C=O stretching of PCBM and PMMA, were adopted to probe the distribution of MA cations, PCBM and PMMA molecules in $MAPbI_3$ films, respectively.

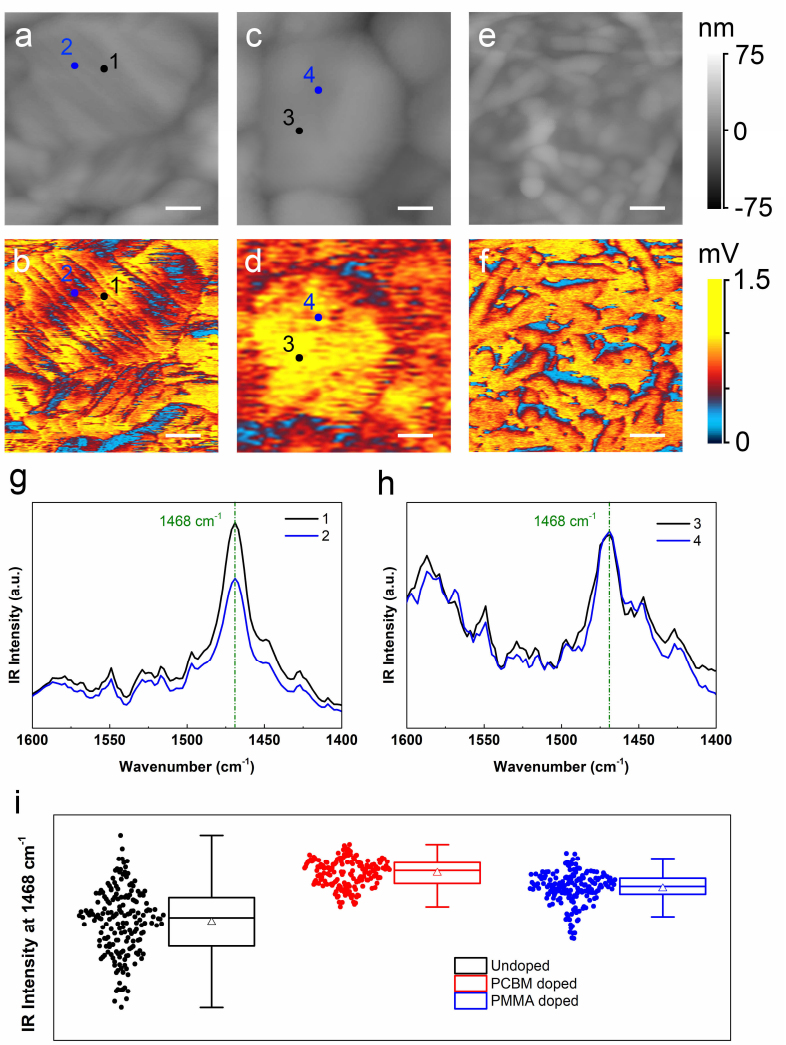


**Fig. S4.** MA distribution in undoped and doped $MAPbI_3$ films by AFM-IR. (a-f) Magnified images of surface topography and chemical distribution for the regions within the boxes of the undoped (a,b), PCBM doped (c,d) and PMMA doped (e,f) $MAPbI_3$ films in Figs. 3a-f, respectively. The scale bars are 100 nm. (g,h) Localized IR spectra from the representative sites marked in Figs. S4a-d. (i) Statistical diagram of the IR intensity at 1468 $cm^{-1}$ sampled from 182 sites for each doping cases. The IR data are shown as solid circles. The boxplots show the maximum, upper quartile, median, lower quartile and minimum from top to bottom, respectively. The mean values are depicted as hollow triangles.

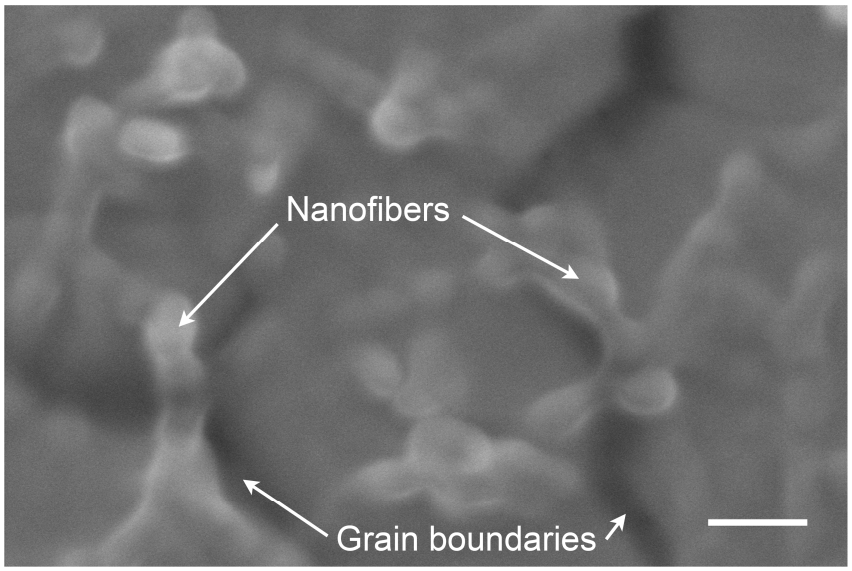


**Fig. S5.** High-resolution SEM image of PCBM+PMMA doped $MAPbI_3$ film. The scale bar is 100 nm.

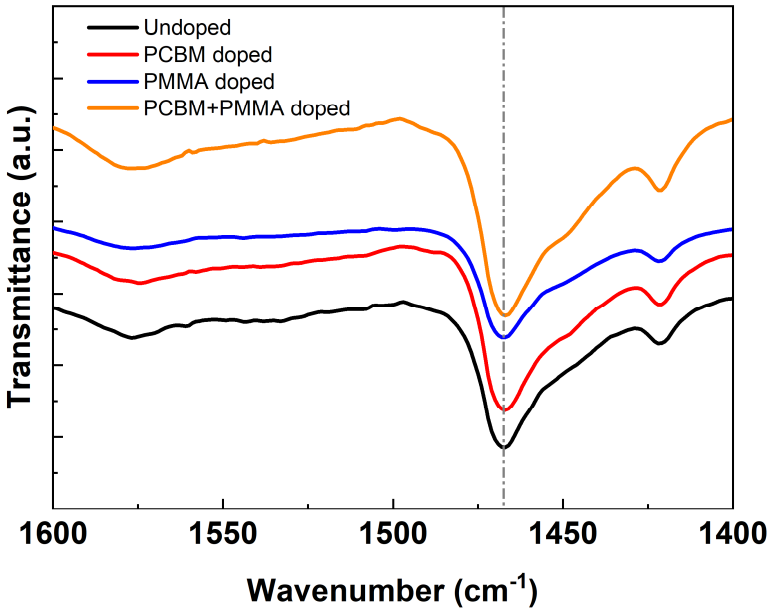


**Fig. S6.** FTIR spectra of undoped, PCBM doped, PMMA doped and PCBM+PMMA doped $MAPbI_3$ films. The representative IR peaks at 1468 $cm^{-1}$ marked by the dash-dot line corresponds to the C-H bending of MA cations in $MAPbI_3$.

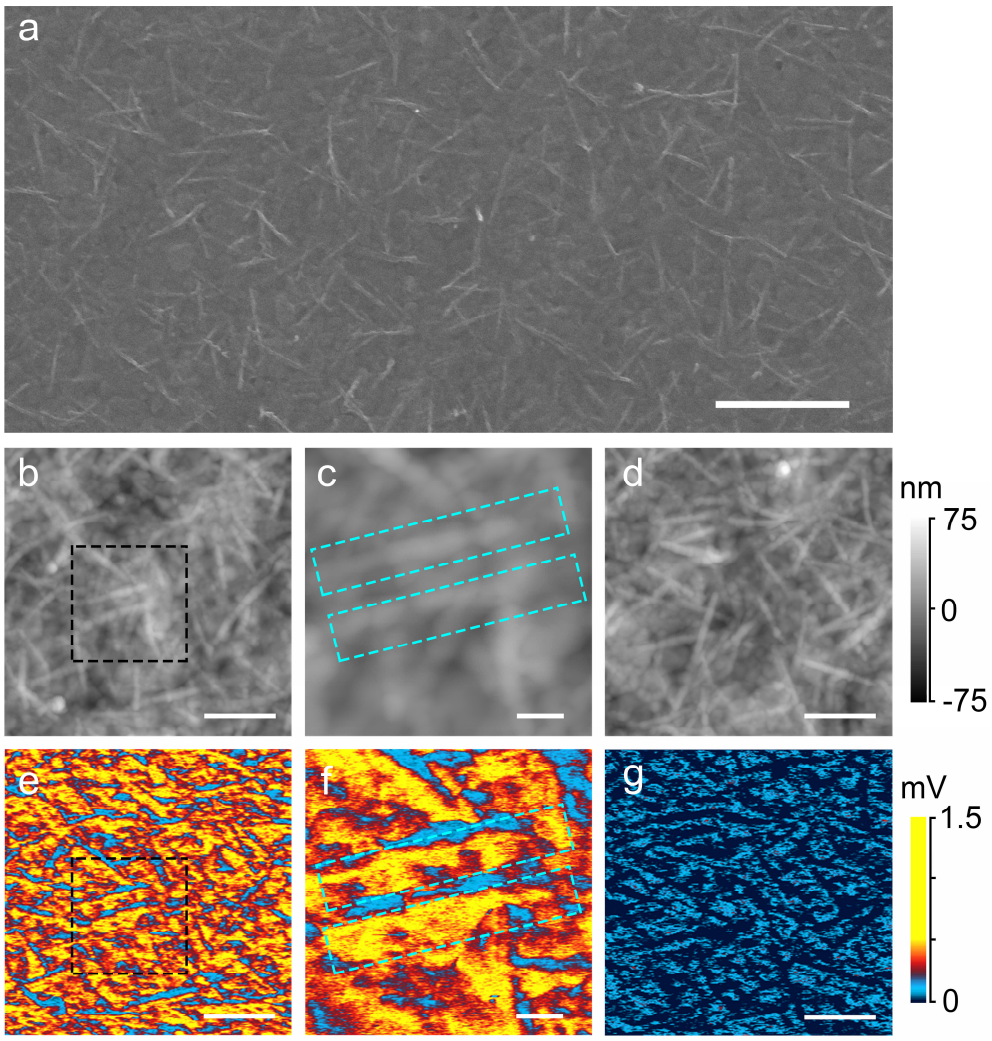


**Fig. S7.** Surface topography and chemical distribution of PMMA doped $MAPbI_3$ films after 20-times CB washing. (a) SEM image of surface topography. (b-g) AFM-IR images of surface topography (b-d) and chemical distribution (e-g). (e) and (f) are the MA mappings corresponding the regions of (b) and (c), respectively. (c) and (f) magnify the same region within the black dashed boxes in (b) and (e). Two parallel nanofibers are highlighted by blue dashed boxes in the magnified images of (c) and (f). (g) is the PMMA mapping corresponding to the region in (d). The size bars are 1 μm (a), 500 nm (b,d,e,g) and 100 nm (c,f).

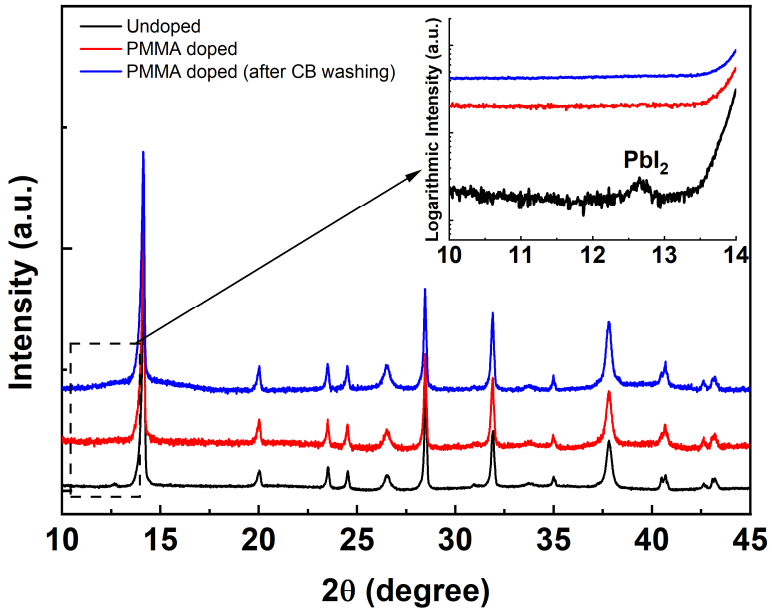


**Fig. S8.** XRD patterns of PMMA doped $MAPbI_3$ films before and after CB washing. The black, red and blue curves are the XRD patterns of the undoped $MAPbI_3$ film, the PMMA doped $MAPbI_3$ film before CB washing and the PMMA doped $MAPbI_3$ film after CB washing, respectively. The inset magnifies the range of $2\theta$ from $10^o$ to $14^o$ within the dashed box.

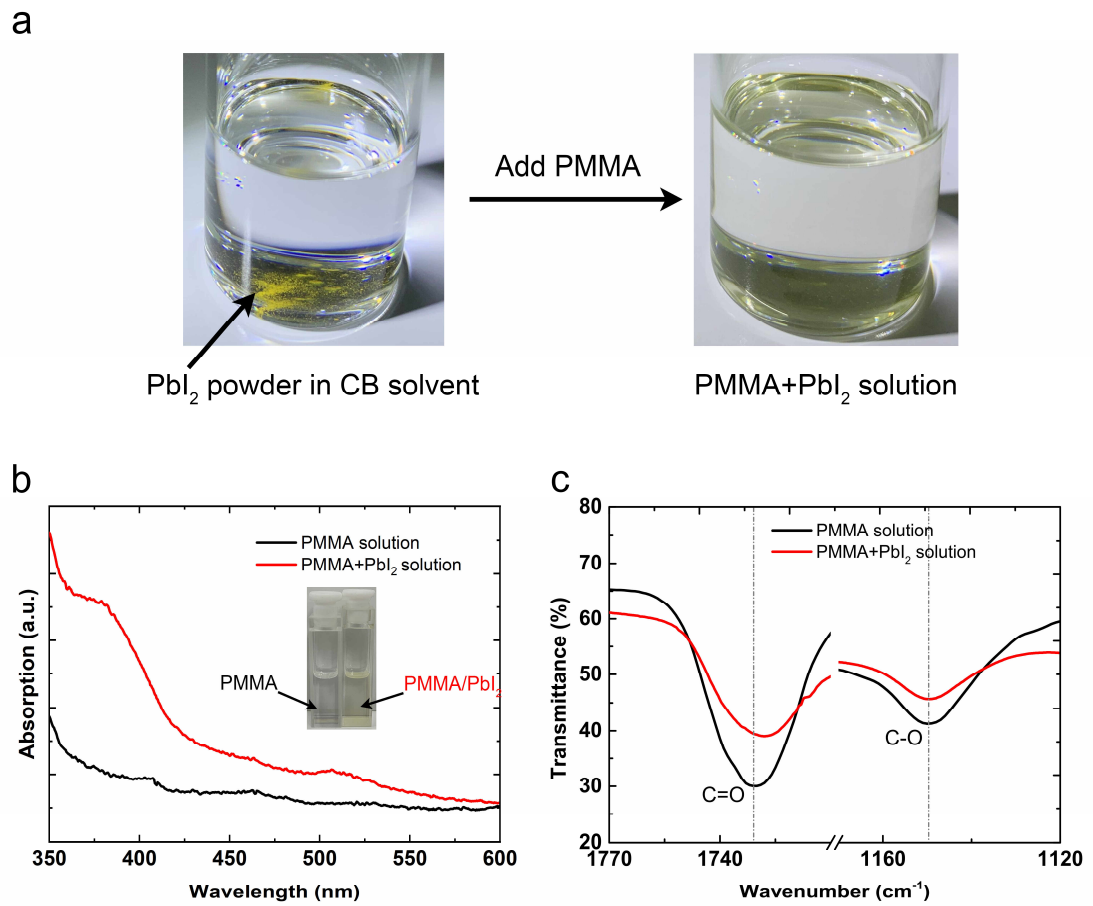


**Fig. S9.** Dissolution of PMMA-$PbI_2$ adducts in CB solvent. (a) Adding PMMA into the CB with the sediment of $PbI_2$ powder. The $PbI_2$ sediment disappears in the CB solvent added by PMMA. (b) UV-Vis absorption spectra of PMMA and PMMA+$PbI_2$ solutions. The PMMA solution represents the solution in which the PMMA dissolves in CB solvent. The PMMA+$PbI_2$ solution is the solution shown on the right of (a) in which the PMMA is added into the CB solvent with the $PbI_2$ sediment fully dissolved. The inset shows the PMMA and PMMA+$PbI_2$ solutions in quartzose cuvettes. Comparing with the case of the PMMA solution (black curve), the UV-Vis absorption spectrum of the PMMA+$PbI_2$ solution (red curve) shows a $PbI_2$ featured adsorption edge at ~450 nm, which proves the existence of $PbI_2$ in the PMMA+$PbI_2$ solution. (c) FTIR spectra of the PMMA and PMMA+$PbI_2$ solutions measured by using the corresponding solutions. The IR peaks of C=O bonds shift while the IR peaks of C-O bonds remain unchanged, which indicates that the $PbI_2$ can form adducts with PMMA and can be dissolved in CB solvent.

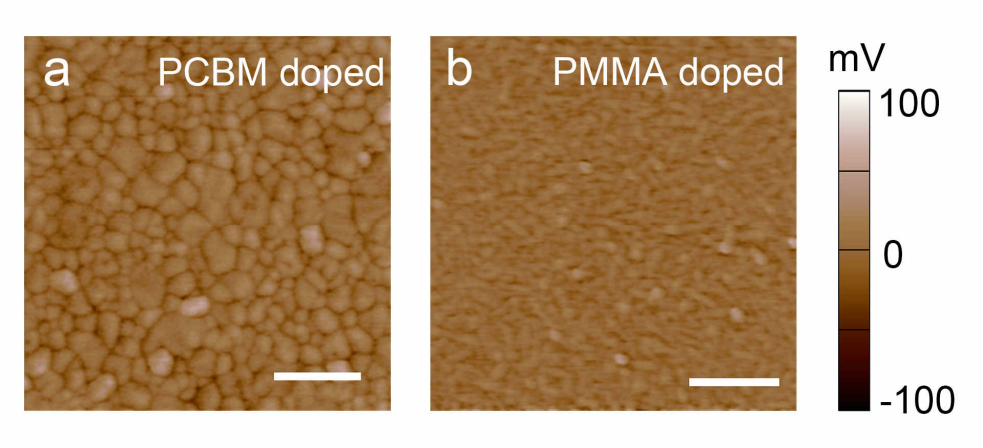


**Fig. S10.** Surface potential distribution of PCBM doped (a) and PMMA doped (b) $MAPbI_3$ films by SKPM. The scale bars are 1 μm.

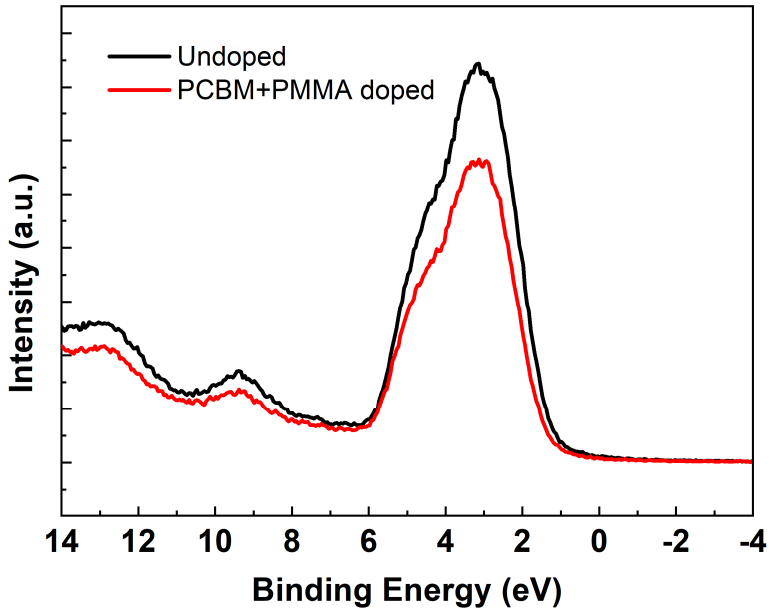


**Fig. S11.** Full-range XPS valance band spectra of undoped and PCBM+PMMA doped $MAPbI_3$ films. Fig. 7c magnifies the range from 4 eV to -1 eV.

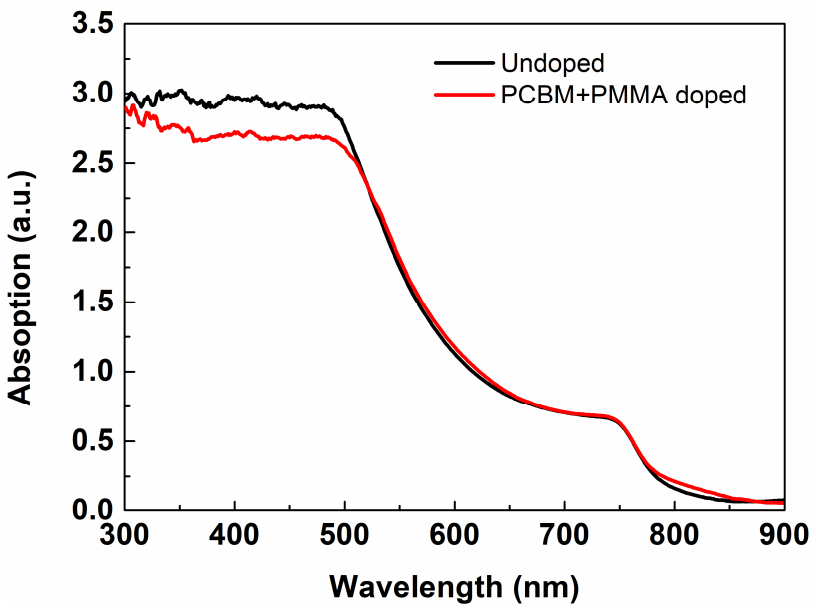


**Fig. S12.** UV-Vis absorption spectra of undoped and PCBM+PMMA doped $MAPbI_3$ films. The undoped and doped $MAPbI_3$ films show the same absorption edges at ~800 nm corresponding to the optical band gap of ~1.55 eV.

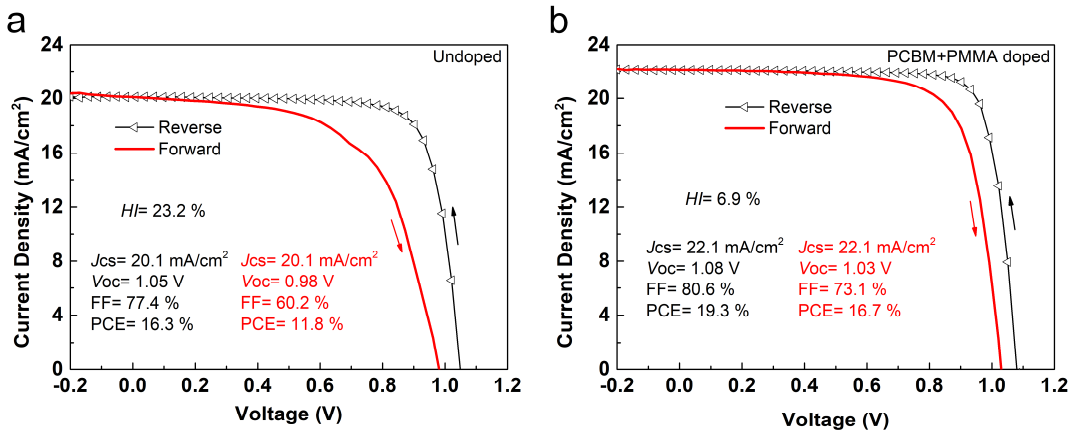


**Fig. S13.** *J-V* characteristics with reverse and forward scans for PSCs based on undoped (a) and PCBM+PMMA doped (b) $MAPbI_3$ films. The reverse mode scans from 1.2 V to -0.2 V, while the forward mode scans from -0.2 V to 1.2 V. $J_{sc}$, $V_{oc}$, FF and PCE denote short current density, open-circuit voltage, fill factor and photoelectric conversion efficiency, respectively. The hysteresis index (*HI*) was calculated[10] by $HI = (J_R(0.8V_{oc})-J_F(0.8V_{oc}))/(J_R(0.8V_{oc}))$, where $J_R(0.8V_{oc})$ and $J_F(0.8V_{oc})$ represent the $J_{sc}$ at 80 % of $V_{oc}$ at the reverse and forward scans, respectively.

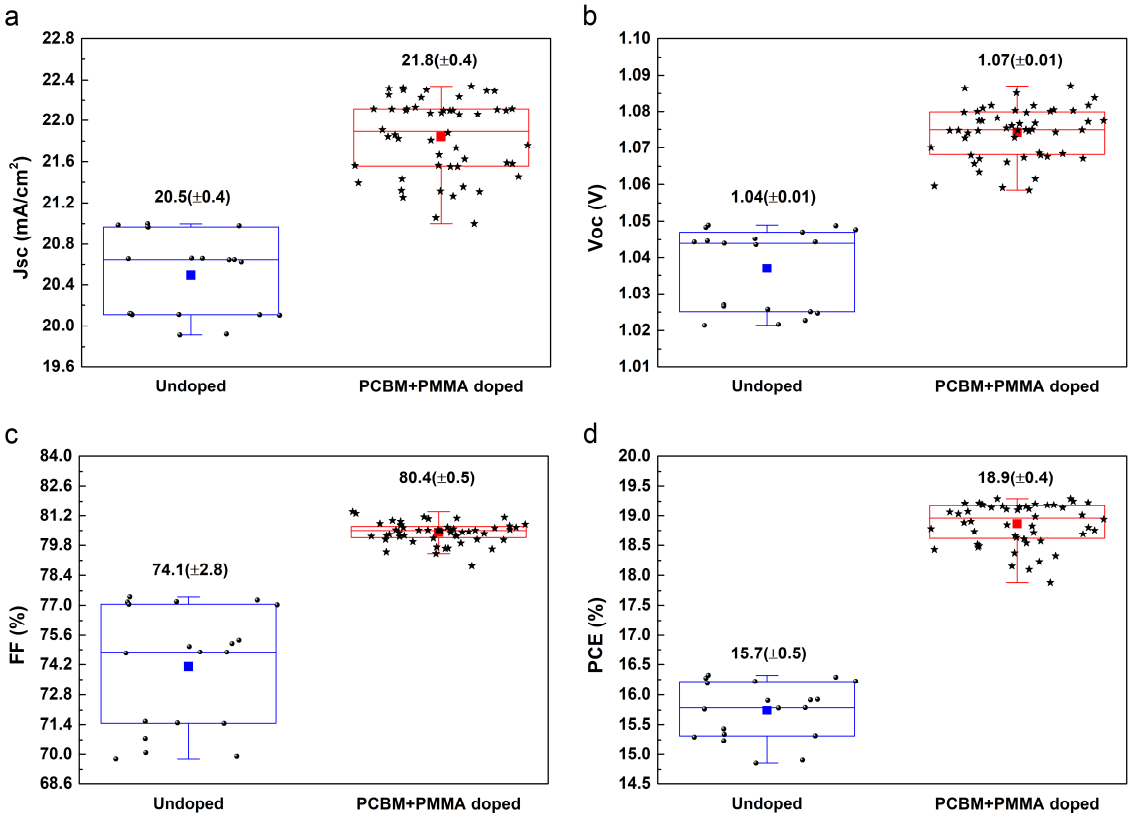


**Fig. S14.** Statistics of photovoltaic performance for PSCs based on undoped and PCBM+PMMA doped $MAPbI_3$ films. (a) $J_{sc}$. (b) $V_{oc}$. (c) FF. (d) PCE. Data for PSCs based on undoped and PCBM+PMMA doped $MAPbI_3$ films are shown as solid circles and stars, respectively. The boxplots show the maximum, upper quartile, median, lower quartile and minimum from top to bottom, respectively. The mean values are depicted as solid squares.

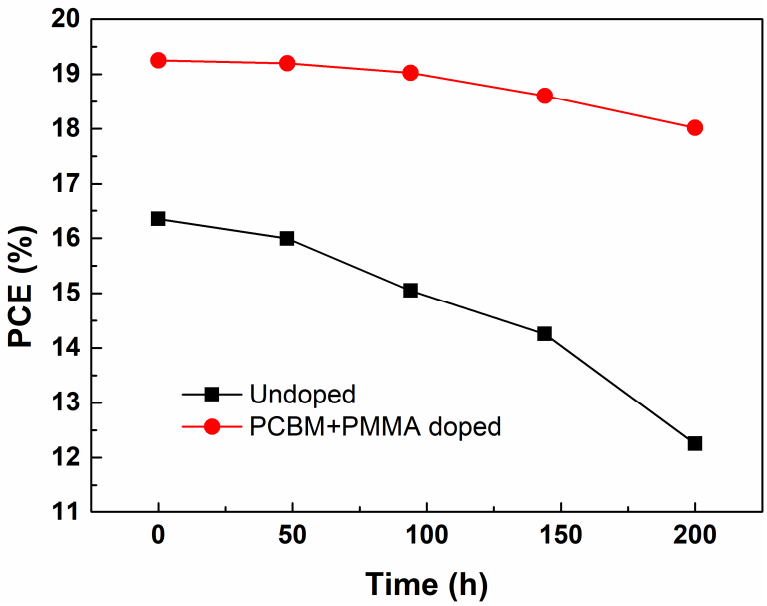


**Fig. S15.** Stability of unencapsulated PSCs based on undoped and PCBM+PMMA doped $MAPbI_3$ films. PCE evolution under ambient atmosphere with relative humidity (RH) of 60-70% without encapsulation.

## Supplementary References


1. J. Burschka, N. Pellet, S.-J. Moon, R. Humphry-Baker, P. Gao, M. K. Nazeeruddin and M. Grätzel, *Nature*, 2013, **499**, 316-319.
2. G. Kresse and J. Furthmüller, *Comput. Mater. Sci.*, 1996, **6**, 15-50.
3. P. E. Blöchl, *Phys. Rev. B*, 1994, **50**, 17953-17979.
4. J. P. Perdew, K. Burke and M. Ernzerhof, *Phys. Rev. Lett.*, 1996, **77**, 3865-3868.
5. S. Grimme, J. Antony, S. Ehrlich and H. A. Krieg, *J. Chem. Phys.*, 2010, **132**, 154104.
6. S. Grimme, S. Ehrlich and L. Goerigk, *J. Comput. Chem.*, 2011, **32**, 1456-1465.
7. Y. Zheng, Y. Jiao, Y. Zhu, L. H. Li, Y. Han, Y. Chen, A. Du, M. Jaroniec and S. Z. Qiao, *Nat. Commun.*, 2014, **5**, 3783.
8. N. W. Chase, https://janaf.nist.gov/, 1998.
9. T. Baikie, Y. Fang, J. M. Kadro, M. Schreyer, F. Wei, S. G. Mhaisalkar, M. Graetzeld and T. J. White, *J. Mater. Chem. A*, 2013, **1**, 5628-5641.
10. H.-S. Kim and N.-G. Park, *J. Phys. Chem. Lett.*, 2014, **5**, 2927-2934.